Synthesis, Characterization, and DFT Calculation of Some New Pyrimidine Derivatives and Theoretical Studies on the Corrosion Inhibition Performance

Esvet, Akbas*[+]; Adem, Ruzgar

Department of Chemistry, Faculty of Science, University of Van Yuzuncu Yil, Van, TURKEY

Cagla, Akbas

Faculty of Pharmacy, University of Inonu, Malatya, TURKEY

Ertan, Sahin

Department of Chemistry, Ataturk University, 25240 Erzurum a, TURKEY

ABSTRACT: *In this study, 5-benzoyl-6-phenyl-4- (4- (trifluoromethoxy) phenyl) - 1,2,3,4-tetrahydroxypyrimidine (**1**); 5-benzoyl-6-phenyl-4- (4- (trifluoromethoxy) phenyl) -1,2,3,4-tetrahydrothioxypyrimidine (**2**) and 5-benzoyl-6-phenyl-4- (3,5-dimethoxy) phenyl) -1,2,3,4-tetrahydrothioxypyrimidine (**3**) compounds were prepared via Biginelli condensation reaction using Metal-organic framework (MIL-101) as an active catalyst. It was established to be an active heterogeneous catalyst for a three-component Biginelli condensation reaction with good yields (75-80 %). Moreover, the catalyst could easily be recovered and recycled without any significant loss of its catalytic activity. Also the compounds 5-benzoyl-6-phenyl-3-acetyl-4-(4-hydroxyphenyl)-1,2,3,4-tetrahydrothioxypyrimidine (**4**) and 5-benzoyl-6-phenyl-3-acetyl-4-(4-trifluoromethoxy)phenyl)-1,2,3,4-tetrahydrothioxypyrimidine (**5**) were obtained acetylation reaction. The structures were characterized on the basis of ^{1}H-NMR, ^{13}C-NMR, FT-IR, and elemental analysis. And also molecular characterizations of compound **4** were analyzed by X-ray crystal analysis. In addition, the corrosion inhibition activity of synthesized compounds was examined with theoretical calculation using DFT method at the level of B3LYP / 6-31G (d, p).*

KEYWORDS: *Tetrahydropyrimidines; Biginelli; X-ray crystal analysis; DFT.*

INTRODUCTION

The one-pot multicomponent cyclo condensation reaction has become a remarkable area of research, particularly in organic chemistry. The one-pot character furnishes fewer by-products in comparison to classical a stepwise synthetic route with lower cost, time, and energy. Among the multicomponent reactions, Biginelli is one of the most studied reactions. It is possible to obtain pyrimidine-derived compounds in good yield with

***** *To whom correspondence should be addressed.*
+ E-mail: esvakbas@hotmail.com
1021-9986/2022/5/1643-1656 14/$/6.04

with Biginelli reaction [1-7]. A large number of pyrimidine-derived are biologically important as antagonists, antihypertensive agents, significant calcium channel blockers, and neuropeptide antagonists [8-10]. Various classical methods are available for the synthesis of pyrimidines employing Lewis acids [11,12]. Heteropolyacids are also used as an acid catalyst for this transformation [13]. MIL-101 (Materials of the Institut Lavoisier no. 101) is a mesoporous Metal-Organic Framework (MOF). The MOF provides many advantages improving molecular accessibility which has a relatively low surface, facile catalyst recovery, recycling, etc. The MIL-101 exhibits good catalytic performance in the esterification reaction of n-butanol with acetic acid in the liquid phase [14], Knoevenagel condensation [14], oxidative desulfurization [15], selective oxidation of alkenes with aqueous hydrogen peroxide [16], hydrolysis and esterification reaction [17] and Biginelli reaction [18]. We have studied its catalytic activity in the Biginelli reaction. The catalyst is easily recoverable and reused up to three times without significant loss of its activity. Hence, short reaction time, facile recovery, and recycling of the catalyst make our process more advantageous to that of the other processes. So in continuation of our previous work [19], and our long-term interest in the synthesis of biologically important pyrimidine derivatives, herein we report the synthesis of new pyrimidine derivatives.

The wide variety of biological activities observed for these compounds turned pyrimidine derivatives into environmentally benign compounds. The requirement for a good corrosion inhibitor, *i.e.* organic compounds which can donate electrons to the unoccupied d-orbital of the metal surface to form coordinate covalent bonds and can also accept free electrons from the metal surface by using their anti-bonding orbital to form feedback bonds, which is also fulfilled by the pyrimidine molecule. Hence pyrimidine derivatives are expected to be excellent corrosion inhibitors at the industrial level, not only due to their efficiency but also due to their non-toxic nature [20].

Acidic environments are widely used in several industrial operations, such as oil well acidification, acid pickling, acid cleaning, and acid descaling, which generally lead to serious metallic corrosion. Despite the relatively limited corrosion resistance of carbon steel, it is widely used in marine applications, chemical processing, petroleum production and refining, construction, and metal-processing equipment due to its excellent mechanical properties and low cost. Out of several methods, the usage of corrosion inhibitors is one of the most important techniques for controlling corrosion. Many organic inhibitors have been tried for the corrosion inhibition of steel, out of which organic compounds with more than one heteroatom-containing π-electrons are found to exhibit high inhibiting properties by providing electrons that interact with metal surfaces [21]. However, the use of several heterocyclic inhibitors has caused negative effects on the environment because of their toxicity and nonbiodegradability. In this context, pyrimidine derivatives are found to attract great interest due to their environmentally benign properties [22].

Quantum Chemical Calculations (QCCs) have been widely used in the reactivity of organic compounds for corrosion inhibition [23]. In this work, the theoretical calculations for the inhibition potentials were explained using QCCs based on Density Functional Theory (DFT). The E_{HOMO} and E_{LUMO} energies of the molecules were calculated in the Gaussian 09 [24].

The effectiveness of an inhibitor can be related not only in its spatial molecular structure but also in its molecular electronic structure. According to frontier orbital theory, the reaction of reactants mainly occurred on Highest Occupied Molecular Orbital (HOMO) and Lowest Unoccupied Molecular Orbital (LUMO), and the formation of a transition state is due to an interaction between the frontier orbitals of the reactants. So, it was important to investigate the distribution of HOMO and LUMO for the exploration of inhibition mechanisms. Organic substances with a higher energy level of HOMO easily donate electrons from HOMO to an empty orbital of appropriate acceptors and E_{LUMO} denotes the ability of the molecule to accept electrons.

The difference between E_{LUMO} and E_{HOMO} energies is called the energy gap (ΔE). It was generally acknowledged that low values of ΔE will provide good inhibition efficiency because the energy for removing an electron from the last occupied orbital will be low [25].

For the theoretical calculation of the inhibitory effect of a molecule, it is necessary to know the ionization potential (I), the electron affinity (A), the chemical hardness-softness (S), the global electrophilicity index (ω), the interaction between the transmitted electron fraction

index (ΔN) and the interaction between back donations. All these values were calculated according to *Shojaie et al.* [26].

EXPERIMENTAL SECTION

Melting points were determined on an Electrothermal Gallenkamp apparatus and are uncorrected. Microanalyses have been performed on LECO CHNS 932 Elemental Analyzer. The FT-IR spectra were obtained as potassium bromide pellets using a Mattson 1000 FTIR spectrometer. The ^{1}H and ^{13}C-NMR spectra were recorded on Bruker 400 MHz spectrometers, using TMS as an internal standard. All experiments were followed by TLC using DC Alufolien Kieselgel 60 F 254 Merck and Camag TLC lamp (254/365 nm).

General procedure for synthesis compounds (1-3).

A mixture of 1.6 mmol dibenzoylmethane, 1.1 mmol arylaldehyde, 1.1 mmol urea for **1, 3,** or thiourea for **2** and 20 mL of glacial acetic acid containing a catalytic amount of MIL-101 (0.01g) was heated under reflux for 12 h. The reaction was cooled to room temperature and the resulting suspension was filtered off and recrystallized from suitable solvents.

Data for the Compounds 1-3

Compound 1: Yield 75%, mp 216-217^{0}C. FTIR (KBr/cm^{-1}) 3217 and 3120 (NH), 1608 (benzoyl) and 1562 (C=O, C=N "tautomer"). ^{1}H-NMR (400 MHz DMSO$_{d6}$, δ/ppm) δ 10.4(s, 1H, N3H), 9.8 (s, 1H, N1H), 8.4- 7.3 (m, 14H, H$_{arom.}$), 5.4 (s, 1H, C4H). ^{13}C-NMR (DMSO$_{d6}$, δ/ppm) δ 195.6, 167.0, 166.4, 152.4, 148.7, 145.4, 139.4, 138.8, 135.6, 134.6, 133.7, 133.2, 130.6, 129.2, 128.7, 126.8, 111.7, 55.1. Anal. Calcd. For $C_{24}H_{17}F_3N_2O_3$: C, 65.75; H, 3.91; N, 6.39. Found: C, 65.74; H, 3.90; N, 6.40.

Compound 2: Yield 80%, mp 202-203^{0}C. FTIR (KBr/cm^{-1}) 3178 and 3105 (NH), 1639 (C=O), 1257 (C=S). ^{1}H-NMR (400 MHz DMSO$_{d6}$, δ/ppm) δ 10.9(s, 1H, N3H), 10.0 (s, 1H, N1H), 8.4- 7.0 (m, 14H, H$_{arom.}$), 5.4 (s, 1H, C4H). ^{13}C-NMR (DMSO$_{d6}$, δ/ppm) δ 196.4, 176.3, 165.4, 153.4, 149.7, 147.4, 140.4, 138.8, 135.6, 134.6, 133.7, 133.2, 130.6, 129.2, 128.7, 126.8, 111.7, 56.1. Anal. Calcd. For $C_{24}H_{17}F_3N_2O_2S$: C, 63.43; H, 3.77; N, 6.16. Found: C, 63.42; H, 3.76; N, 6.17.

Compound 3: Yield 78%, mp 220-221^{0}C. FTIR (KBr/cm^{-1}) 3232 and 3109 (NH), 1701 and 1627 (C=O). ^{1}H-NMR (400 MHz DMSO$_{d6}$, δ/ppm) δ 9.8 (s, 1H, N3H), 8.2 (s, 1H, N1H), 7.0- 7.5 (m, 13H, H$_{arom.}$), 5.7 (s, 1H, C4H), 3.7 (s, 6H, 2CH$_3$). ^{13}C-NMR (DMSO$_{d6}$, δ/ppm) δ 195.6, 176.3, 165.4, 153.4, 149.7, 147.4, 140.4, 138.8, 135.6, 134.6, 133.7, 133.2, 130.6, 129.2, 128.7, 126.8, 111.7, 56.1 (-OCH$_3$). Anal. Calcd. For $C_{25}H_{22}N_2O_4$: C, 72.45; H, 5.35; N, 6.76. Found: C, 72.46; H, 5.36; N, 6.75.

5-benzoyl -6-phenyl -3-acetyl -4-(4-hydroxyphenyl)-1,2,3,4-tetrahydrothioxypyrimidine (4)

A mixture of **6** [19] (1 mmol) was boiled in acetic anhydride (3 mL) for 3 h, then the reaction mixture was allowed to cool to room temperature, poured over crushed ice, and stirred for several minutes. The separated solid was filtered off, washed with water, and recrystallized from 2-prophanol to give compound **4**: Yield 60%, mp 200-202^{0}C. FTIR (KBr/cm^{-1}) 3278 (NH), 1702 and 1645 (C=O), 1258 (C=S). ^{1}H-NMR (400 MHz DMSO$_{d6}$, δ/ppm) δ 10.5 (s, 1H, -OH), 9.7 (s, 1H, NH), 7.4- 6.8 (m, 14H, H$_{arom.}$), 5.4 (s, 1H, C4H), 2.8(s, 3H, CH$_3$). ^{13}C-NMR (DMSO$_{d6}$, δ/ppm) δ 195.2 (C=O$_{benzoyl}$), 178.6 (C=S), 174.3 (C=O), 147.2, 144.4, 138.7, 132.2, 131.8, 131.3, 131.2, 129.8, 128.5, 128.2, 127.9, 126.2, 126.1, 114.8, 55.03, 28.0 (CH$_3$). Anal. Calcd. For $C_{25}H_{20}N_2O_3S$: C, 70.07; H, 4.70; N, 6.54. Found: C, 70.06; H, 4.71; N, 6.55.

5-benzoyl-6-phenyl-3-acetyl-4- (4-trifluoromethoxy) phenyl)-1,2,3,4-tetrahydrothioxy pyrimidine (5)

A mixture of compound **2** (1 mmol) was boiled in acetic anhydride (3 mL) for 3 h, then the reaction mixture was allowed to cool to room temperature, poured over crushed ice, and stirred for several minutes. The separated solid was filtered off, washed with water, and recrystallized from ethanol to give compound **5**: Yield 65%, mp 190-191^{0}C. FTIR (KBr/cm^{-1}) 3240 (NH), 1693 and 1646 (C=O), 1256 (C=S). ^{1}H-NMR (400 MHz DMSO$_{d6}$, δ/ppm) δ 9.8 (s, 1H, NH), 8.5- 7.2 (m, 14H, H$_{arom.}$), 5.6 (s, 1H, C4H), 2.9 (s, 3H, CH$_3$). ^{13}C-NMR (DMSO$_{d6}$, δ/ppm) δ 196.6 (C=O$_{benzoyl}$), 178.3 (C=S), 173.4 (C=O), 153.4, 149.7, 147.4, 140.4, 138.8, 135.6, 134.6, 133.7, 133.2, 130.6, 129.2, 128.7, 127.3, 126.8, 114.3, 56.3. Anal. Calcd. For $C_{26}H_{19}F_2N_2O_3S$: C, 62.90; H, 3.86; N, 5.64. Found: C, 62.91; H, 3.85; N, 5.65.

Crystallography

For the crystal structure determination, single-crystal of compound **4** was used for the data collection on a four-circle Rigaku R-AXIS RAPID-S diffractometer (equipped

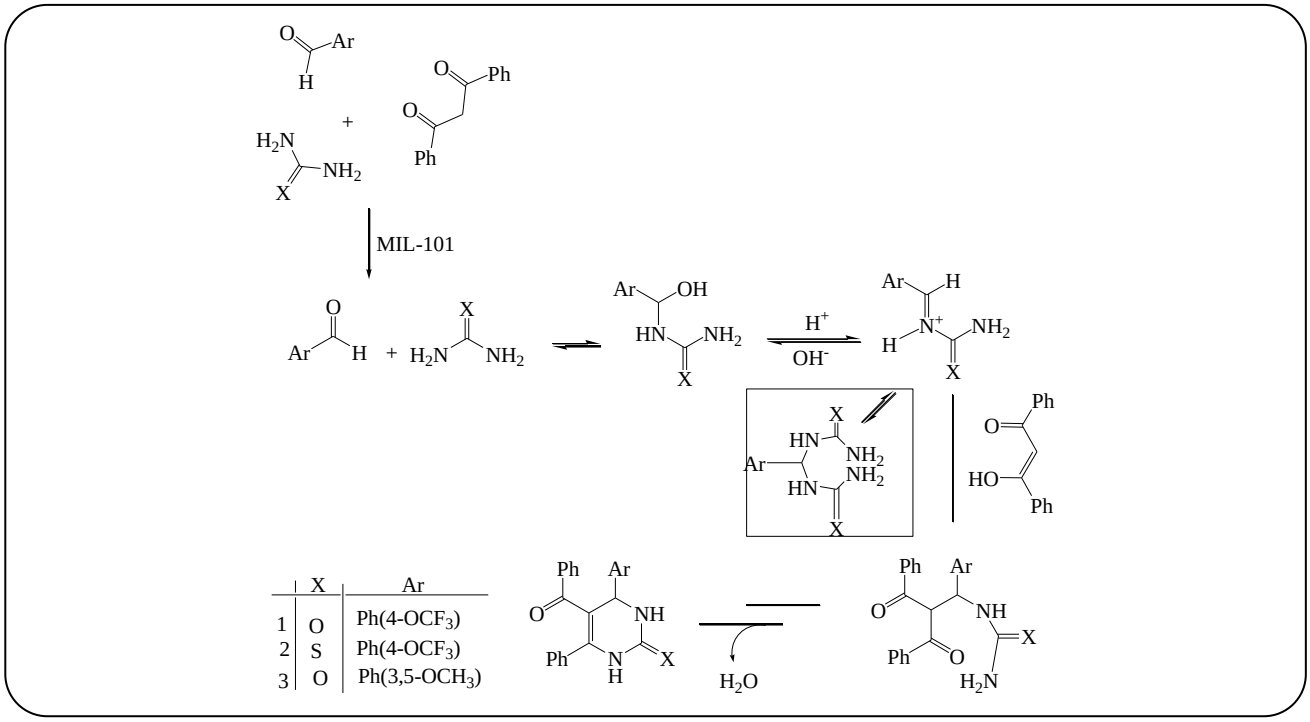

Scheme 1: Obtain compounds 1-3.

with a two-dimensional area IP detector). Graphite-monochromated Mo-K_α radiation (λ = 0.71073 Å) and oscillation scans technique with Δw = 5º for one image were used for data collection. The lattice parameters were determined by the least-squares methods on the basis of all reflections with $F^2 > 2\sigma(F^2)$. Integration of the intensities, correction for Lorentz and polarization effects, and cell refinement was performed using CrystalClear (Rigaku/MSC Inc., 2005) software [27]. The structures were solved by direct methods using SHELXS-97 [28] and refined by a full-matrix least-squares procedure using the program SHELXL-97 [28]. All nonhydrogen atoms were refined anisotropically and H atoms were positioned geometrically and refined using a riding model. The final difference in Fourier maps showed no peaks of chemical significance. *Crystal data for* ***4***: $C_{25}H_{20}N_2O_3S$, crystal system, space group: monoclinic, $P2_1/n$; (no:14); unit cell dimensions: a = 11.207 (2), b = 13.138(2), c = 15.580(3) Å, α= 90, β = 106.768(6), γ = 90º; Volume: 2196.4 (7) Å^3; Z = 4; calculated density: 1.296 g/cm^3; absorption coefficient: 0.176 mm^{-1}; F(000): 896; θ-range for data collection 2.4–29.2º; refinement method: full matrix least-square on F^2; data/parameters: 4470/281; goodness-of-fit on F^2: 1.051; final R-indices [$I > 2\sigma(I)$]: R_1 = 0.078, wR_2 = 0.215; largest diff. peak and hole: 0.240 and -0.280 e Å^{-3}.

Crystallographic data that were deposited in CSD under CCDC-1544962 registration numbers contain the supplementary crystallographic data for this Letter. These data can be obtained free of charge from the Cambridge Crystallographic Data Centre (CCDC) *via* www.ccdc.cam.ac.uk/data_request/cif and are available free of charge upon request to CCDC, 12 Union Road, Cambridge, UK (fax: +441223 336033, e-mail: deposit@ccdc.cam.ac.uk).

RESULTS AND DISCUSSION

Chemistry

The Biginelli reaction is one of the Multicomponent cyclo condensation reactions. There are three possible mechanisms for this reaction. The first mechanism was recommended by *Folkers* in 1933 [29], the second by *Sweet* in 1973 [30], and the latest in 1997 by *Kappe* [31].

In this work, we used the Biginelli reaction with a catalytic amount of MIL-101 to obtain compounds **1-3** (Scheme 1).

MIL-101 (Fig. 1), a kind of Metal-Organic Framework (MOFs), has attracted attention in recent years with its promising applications in the chemical industries. MIL-101 is also known as “Porous Chromium Terephthalate”. It has a very high surface area and pore volume. MIL-101 exhibits exceptional stability against moisture and other

Table 1: The optimization of reaction conditions for compound 1.

Rate of A:B: C:D$_{(mmoles)}$	Solvent	Temp(^{0}C)	Time(h)	Yield (%)(**1**)
1(A):1(B):1(C)	Ethanol	r.t	10	-
1(A):1(B):1(C):0.001(D)	Ethanol	75	6	-
1(A):1(B):1(C):0.01(D)	Ethanol	75	10	10
1(A):1(B):1(C)	Acetic acid	r.t	10	-
1(A):1(B):1(C):0.001(D)	Acetic acid	r.t	10	-
1(A):1(B):1(C):0.001(D)	Acetic acid	110	10	45
1.6(A):1.1(B):1.1(C):0.01(D)	Acetic acid	110	6	75

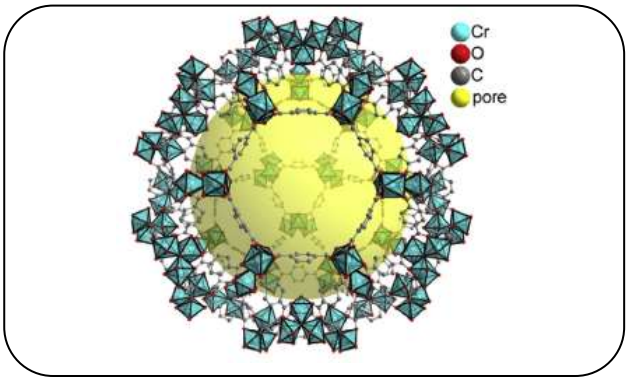

Fig. 1: MIL-101, [$Cr_3F(H_2O)_2O\{O_2CC_6H_4(CO_2)\}_3.nH_2O$].

chemicals. It also consists of coordinately unsaturated Cr- sites with high concentrations are available for catalysis and adsorption applications [32].

In our present protocol, the three-component condensation reaction between aryl aldehyde, dibenzoylmethane, and urea (and thiourea) was carried out using MIL-101 as a catalyst. This protocol gives a good yield to the products. The catalytic efficiency of the heterogeneous MIL-101 catalytic system was monitored. The results of the reactions pointed to the optimized performance of 0.6 mol% of MIL-101.

We chose the reaction of compound **1** as a model reaction to optimize the reaction conditions. A series of experiments were performed to evaluate the feasibility of the formation of pyrimidines. The results were shown in Table 1. It can be said that dibenzoylmethane(A)/ arylaldehyde(B)/urea (or thiourea)(C)/MIL-101(D) (1.6:1.1:1.1: 0.01 mmol) at 110^{0}C in acetic acid are the best result.

Compounds obtained as a result of the Biginelli reaction were characterized on the basis of their spectral data and elemental analyses.

In ^{1}H-NMR spectra of compound **1** showed that δ 10.4 and 9.8 ppm (s, 1H, NH) and 5.4 (s, 1H, C4H). The ^{13}C NMR spectrum of compound **1** revealed signals at δ 195.6 (C=O, benzoyl) and 167.0 ppm (C=O). All other spectral data are in accordance with the proposed structures for compound **1**.

In ^{1}H-NMR spectra of compound **2** showed that δ 10.9 and 10.0 ppm (s, 1H, NH) and 5.4 (s, 1H, C4H). The ^{13}C NMR spectrum of compound **2** revealed signals at δ 196.4 (C=O, benzoyl) and 176.3 ppm (C=S). All other spectral data are in accordance with the proposed structures for compound **2**.

In ^{1}H-NMR spectra of compound **3** showed that δ 9.8 and 8.2 ppm (s, 1H, NH) and 5.7 (s, 1H, C4H). The ^{13}C NMR spectrum of compound **3** revealed signals at δ 195.6 (C=O, benzoyl) and 176.3 ppm (C=O). All other spectral data are in accordance with the proposed structures for compound **3**.

On the other hand, 3-acetyl pyrimidine derivatives **4** and **5** were prepared *via* the reaction of compounds **2** and **6** [19] with acetic anhydride (Scheme 2).

The molecular structure of the 1-[5-benzoyl-6-(4-hydroxyphenyl)-4-phenyl-2-sulfanylidene-3,6-dihydropyrimidin-1(2*H*)-yl]ethan-1-one **(4)** was characterized by single crystal X-ray diffraction analysis (Fig. 2). Novel compound **4** crystallized as a red prism and were solved in the monoclinic space group $P2_1/n$ with four molecules in the unit cell. The structure has hydroxyphenyl, phenyl, benzoyl, ethanone, and sulfur units attached to the pyrimidine core. Molecules **4** form centrosymmetric dimers connected by O3-H···O1 [D···A = 3.398(3) Å] hydrogen bonds. These dimeric units form a polymeric structure with adjacent dimers. The hydrogen bonds N1-H···O2, d(N1···O2) distances of 2.857(3) Å

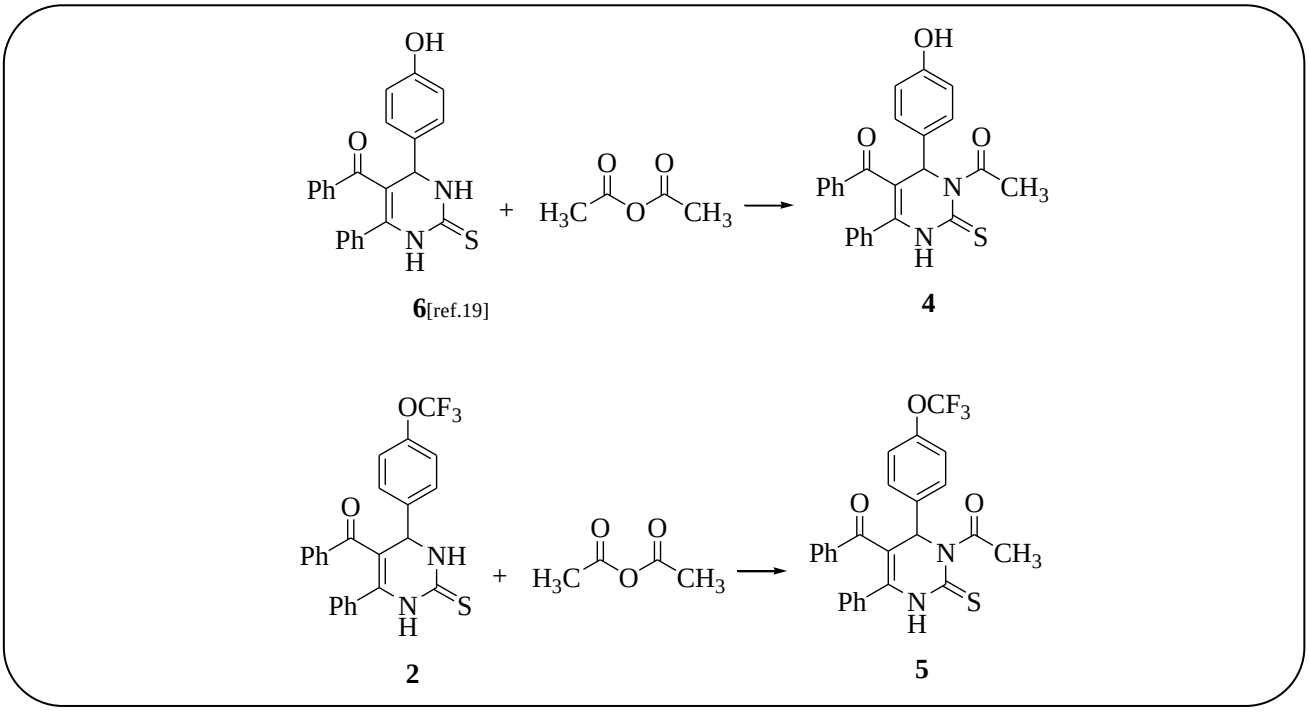

Scheme 2: Synthesis of compounds 4 and 5.

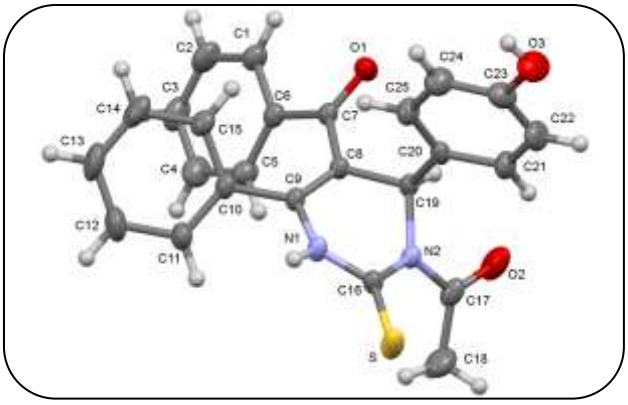

Fig. 2: The molecular structures of compound 4. Displacement ellipsoids are drawn at the 50% probability level.

causes the formation of the 2*D*-polymeric form (Fig. 3). Meanwhile, the π-π stacking interactions between the delocalized π-electrons of the phenyl rings are relatively weak. The distance between the ring centroids is in the range of 4.21–5.52 Å.

Calculation Analysis

All synthesized compounds were performed using GAUSSIAN 09 software [33]. For geometry optimizations, Becke's three-parameter exact-exchange functional (B3), combined with the gradient-corrected correlation functional of Lee–Yang–Parr (LYP) of the density functional theory methods (B3LYP) [34-36] were used with 6-31+G (d, p) basis set. The optimized structures were characterized as true minima by vibrational frequency calculations.

The higher occupied molecular orbital (HOMO) and lowest unoccupied molecular orbital (LUMO) diagrams are illustrated using B3LYP method with 631+G (d, p) basis set in the gas phase in Fig.4 and their E_t, E_{HOMO}, E_{LUMO}, ΔE_{gap} and dipole moment values determined and showed in Table 2.

Very useful information can be obtained by the quantum chemical calculations to examine the corrosion-inhibiting effects of organic compounds. The quantum chemical parameters of all compounds such as μ, IP, A, χ, η, w, S, ΔN, and $\Delta E_{back\ donation}$ were calculated according to *Shojaie. et al.* (Table 3).

The inhibitory effect of a particular compound is usually attributed to the adsorption of the molecule to the metal surface. When the chemisorption occurs, one of the species entering the reaction behaves as an electron pair donor, and the other acts as an electron pair receiver.

The basic state geometry of the inhibitor and the structure of HOMO and LUMO play a role in the activity properties of the inhibitors. Remarkable, the shape

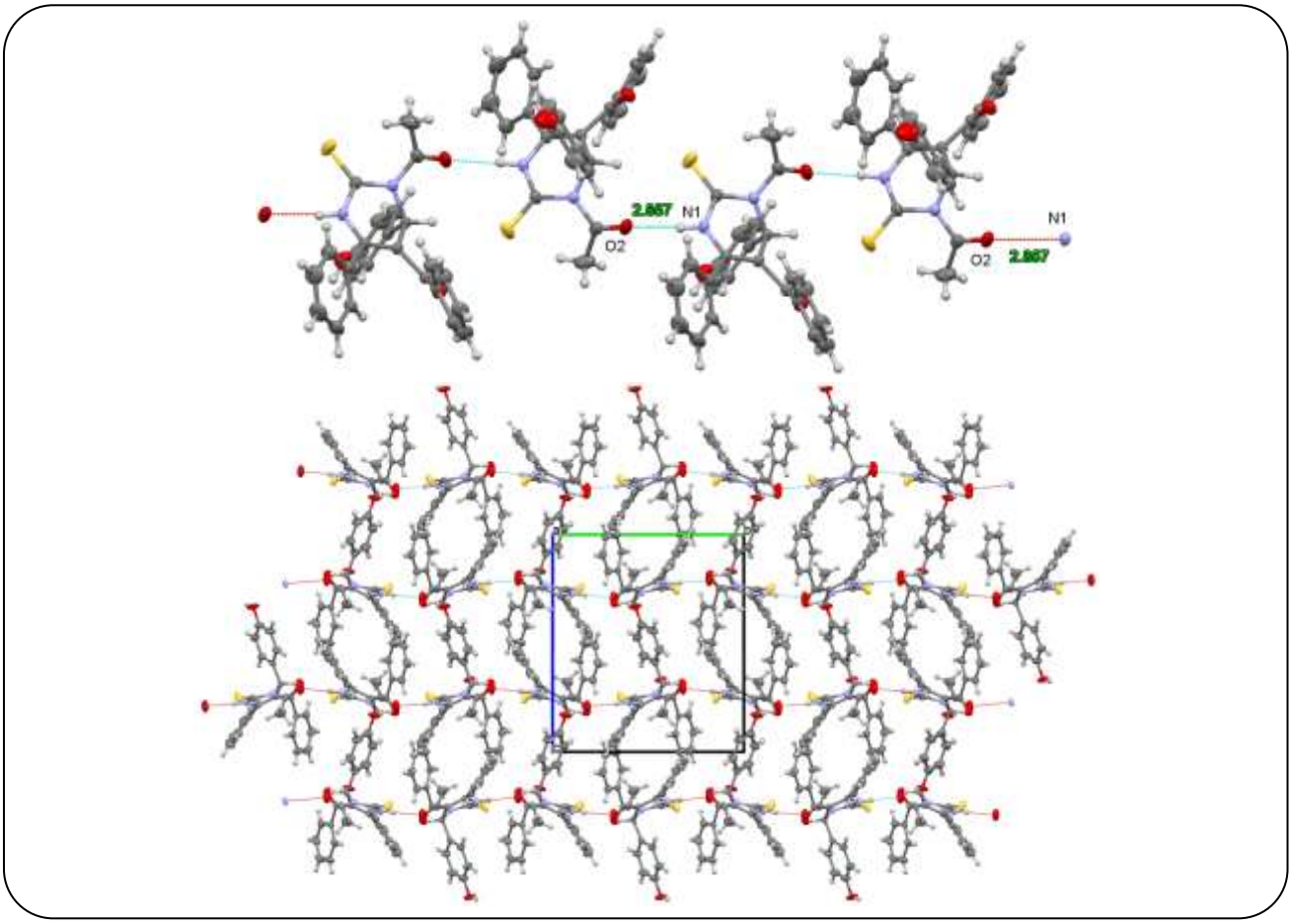

Fig. 3: (Up) Depiction of the N-H···O hydrogen bonds found in (4) that form chains propagating along the [010] direction. (Down) 2D H-bonding geometry with the unit cell viewed down along the a-axis.

of HOMO and LUMO is structurally dependent. The electron density of the HOMO site in the inhibitors examined is often distributed over atoms with delocalized characters, indicating that they are the favorite adsorption domains.

The inhibitors could not only donate electron metal ions to un-emissive d orbitals but can also accept electrons from the d-orbital of the metal, which leads to a feedback bond. The electrons found in the HOMO can easily donate. E_{HOMO} also plays a most important role during the corrosion inhibition course and this is directly related to the ionization potential. Increasing E_{HOMO} leads to a higher inhibition effect.

Another parameter of the molecular structure is the LUMO, which determines the polarizabilities of the compound. The lower the value of E_{LUMO}, the more probable the molecule would accept electrons, and the energy of the LUMO is directly related to the electron affinity.

Similar relations were found between the rates of inhibition and the energy gap. Larger values of the energy gap will provide low reactivity to a molecule. Lower values of the energy gap render good inhibition efficiency because the energy required to remove an electron from the lowest occupied orbital will be low.

Dipole moment (μ_{Debye}) is another important electronic parameter for corrosion inhibitors. The high value of the dipole moment probably increases the adsorption between the chemical compound and the metal surface.

On the other hand, absolute hardness (η), softness (S), global electrophilicity index (ω) electrons transferred (ΔN), and $\Delta E_{back\ donation}$ values are important properties used to measure the stability and reactivity of a molecule (Table 3).

The chemical hardness fundamentally signifies the resistance toward the deformation or polarization of the electron cloud of the atoms, ions, or molecules under small

Table 2. The total energies (E_t), E_{HOMO}, E_{LUMO}, ΔE_{gap} and dipole moment for molecules 1-5.

Compounds	E_t (a.u.)	$E_{HOMO}(eV)$	$E_{LUMO}(eV)$	$\Delta E_{gap}(eV)$	Dipole Moment (Debye)
1	-1559.083009	-5.2040	-2.0112	3.1927	6.480535
2	-1882.031664	-5.2551	-2.0411	3.2139	6.397064
3	-1375.865447	-5.0451	-1.8874	3.1576	4.187706
4	-1697.028044	-5.3732	-3.3277	2.0454	5.665492
5	-2034.739317	-5.1240	-2.1502	2.9737	7.378537

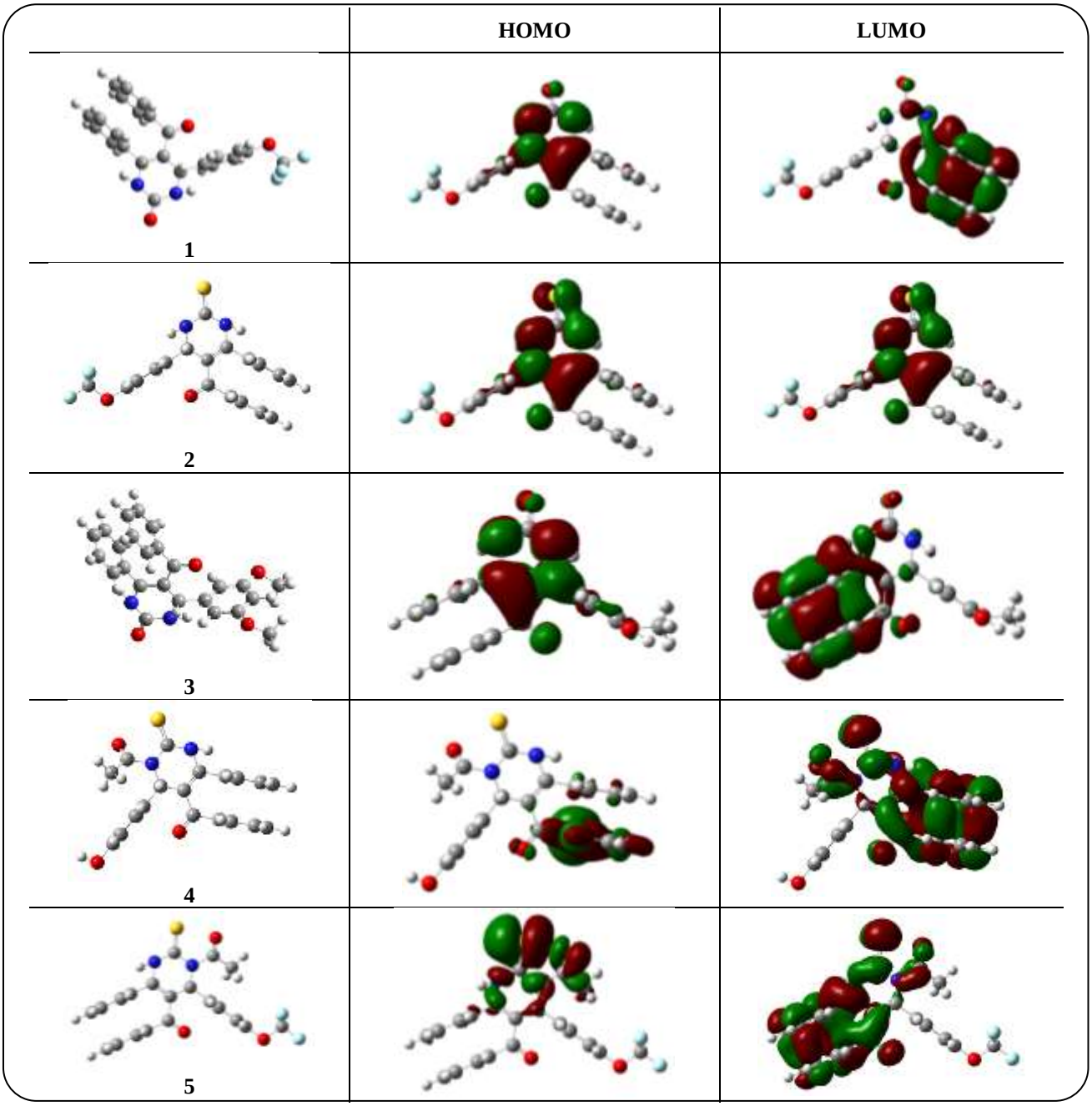

Fig. 4: The optimized structures of molecules 1-5 obtained at B3LYP/631+g(d,p).

Table 3: The quantum chemical parameters for all compounds.

	1	2	3	4	5
Ionization potential "IP(eV)"	5.2040	5.2551	5.0451	5.3732	5.1240
Electron affinity "A(eV)"	2.0112	2.0411	1.8874	3.3277	2.1502
Chemical hardness "η(eV)"	3.1928	3.2140	3.1577	2.0455	2.9738
Chemical softness "S"	0.3132	0.3111	0.3167	0.4889	0.3363
Electronegativity "χ(eV)"	3.6076	3.6481	3.4663	4.3505	3.6371
Transferred electrons fraction "(ΔN)"	0.5313	0.5215	0.5596	0.6496	0.5654
Electrophilicity index "(ω)"	6.5768	6.3663	2.7768	7.8459	9.1537
$\Delta E_{back\ donation}$	-0.7982	-0.8035	-0.7894	-0.5114	-0.7435

perturbation of chemical reaction. A hard molecule has a large energy gap and a soft molecule has a small energy gap.

The global electrophilicity index was introduced by Parr as a measure of energy lowering due to maximal electron flow between donor and acceptor this index measures the propensity of chemical species to accept electrons. A good, more reactive, the nucleophile is characterized by a lower value of μ, ω; and conversely a good electrophile is characterized by a high value of μ, ω. This new reactivity index measures the stabilization in energy when the system acquires an additional electronic charge ΔN from the environment. Thus the fraction of electrons transferred from the inhibitor to the metallic surface.

According to the simple charge transfer model for donation and back-donation of charges, an electronic the back-donation process might be occurring governing the interaction between the inhibitor molecule and the metal surface. The concept establishes that if both processes occur, namely charge transfer to the molecule and back-donation from the molecule, the energy change is directly proportional to the hardness of the molecule.

The $\Delta E_{back\ donation}$ implies that when $\eta > 0$ and $\Delta E_{back\ donation} < 0$ the charge transfer to a molecule, followed by a back donation from the molecule, is energetically favored. In this context, hence, it is possible to compare the stabilization among inhibiting molecules, since there will be an interaction with the same metal, then, it is expected that it will decrease as the hardness increases [37-45].

According to the calculations, compounds **4** and **5** appear to be good inhibitors for corrosion.

Non-linear Optical (NLO) properties

The non-linear optical properties of molecules **1-5** were calculated using the B3LYP/6-31+G(d, p) method in the gas phase. The total dipole moment μ_{tot}, mean polarizability (αtot), and the average value of the first hyperpolarizability (β_{tot}) can be calculated using the following equations.

$$\mu_{tot} = \mu_x^2 + \mu_y^2 + \mu_z^2$$

$$\alpha_{tot} = \left(\alpha_{xx} + \alpha_{yy} + \alpha_{zz} \right) / 3$$

$$\beta_{tot} = \left[\left(\beta_{xxx} + \beta_{xyy} + \beta_{xzz} \right)^2 + \left(\beta_{yyy} + \beta_{yxx} + \beta_{yzz} \right)^2 + \left(\beta_{zzz} + \beta_{zxx} + \beta_{zyy} \right)^2 \right]^{1/2}$$

The calculated values and related components are given in Table 4. For more active NLO properties, the higher values of dipole moment, molecular polarizability, and hyperpolarizability are important. According to the results, molecules **2** and **5** with the highest hyperpolarizabilities have more active NLO properties than the others.

The calculated values and related components are given in Table 4. For more active NLO properties, the higher values of dipole moment, molecular polarizability, and hyperpolarizability are important. According to the results, molecules **3** and **4** with the highest hyperpolarizabilities have more active NLO properties than the others.

The geometrical parameters (bond lengths, bond angles, and dihedrals) were calculated for molecule **1** (Table 5) following the atom numbering scheme given in Fig. 5.

Molecular Electrostatic Potentials (MEPs)

It is well known that the molecular electrostatic potential (MEP) provides information about reactive sites

Table 4: Electric dipole moment μ, polarizability α and first hyperpolarizability β obtained for molecules 1-5 by B3LYP level with the 6-31+G (d, p) basis set.

Parameters (a.u)	1	2	3	4	5
β_{xxx}	21.9952	18.2324	70.8298	57.3553	-29.1977
β_{xyy}	-26,4910	-25.3353	7.3981	10.1086	14.6965
β_{xzz}	-14.3665	-15.2244	-3.7685	-16.7916	13.2682
β_{yyy}	-65,5949	-64.1935	-64.9665	-85.2256	-62.1871
β_{yxx}	-17,1444	-24.4920	-29.8154	0.7259	-24.8174
β_{yzz}	-3.3103	-8.18329	1.8575	-9.4992	-8.9190
β_{zzz}	0.1742	0.22261	0.2308	3.7245	0.8950
β_{zxx}	-0,3869	-0.38493	0.2804	-3.1321	-1.2202
β_{zyy}	-0.6538	-0.71710	0.2435	-2.7876	-5.3863
β_{tot} (esu) 10^{-33}	761.1007	858.8544	1028.7557	922.7603	830.2479
α_{xx}	-61.7917	-65.3764	-46.8762	-69.2149	-70.4216
α_{yy}	-87.6218	-90.1952	-86.9597	-77.3413	-98.8615
α_{zz}	-63.5994	-66.8475	-66.1957	-70.1375	-73.3945
α_{tot} (esu) 10^{-33}	-613.4277	-640.5148	-576.0454	-624.0281	-698.8560
μ_x	2.0393	1.9516	-0.4521	1.8042	-2.3586
μ_y	-1.5310	-1.5898	-1.5844	-2.2944	-1.6413
μ_z	-0.0209	-0.0210	0.0244	0.7974	-0.4163
μ_{tot} (esu) 10^{-33}	2.55013	2.51727	1.6478	3.0259	2.9035

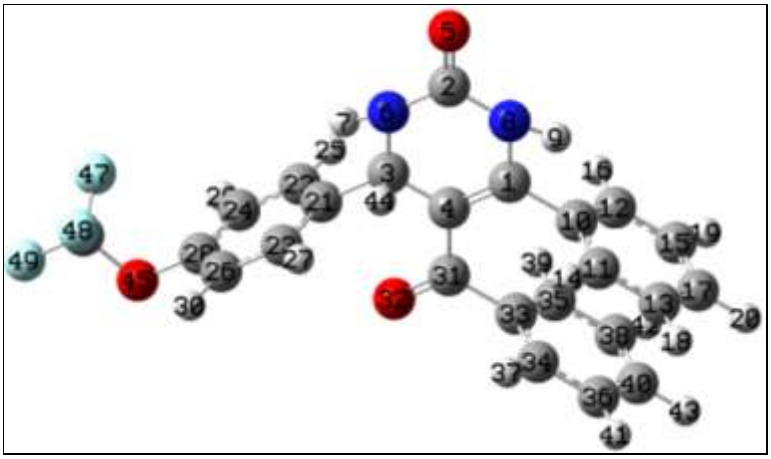

Fig. 5: The atom numbering for molecule 1.

Table 5. The calculated values are of selected bond lengths (Å), angles (º), and dihedrals (º) for molecule 1. The calculated values are given for the gas phase.

	Bond lengths	Bond Angles	Dihedral Angles
C(4)(1,3,2)	1.3948292	30.0036507	178.9641441
O(5)(2,1,4)	1.2584001	150.0137783	179.9619213
N(6)(3,1,4)	1.3948252	90.0083836	179.9674314
H(7)(6,3,1)	1.0000001	66.2257267	169.2577089
N(8)(2,1,4)	1.3947122	30.0009942	-179.9719853
H(9)(8,2,1)	1.0000001	168.5444773	120.6148450
C(10) (1,4,3)	1.5400001	120.0043196	-179.9798413
C(31)(4,1,8)	1.5400001	120.0079967	179.9891754
O(32) (31,4,1)	1.2584001	120.2269461	-180.0000000
H(44) (3,1,4)	1.0700001	90.0132439	89.9742219
O(45) (28, 26,23)	1.4300001	120.0248586	-179.9563255
C(46)(45,28,26)	1.4300001	109.5000004	89.7787921
F(47) (46,45,28)	1.3500001	109.4712303	59.7921488

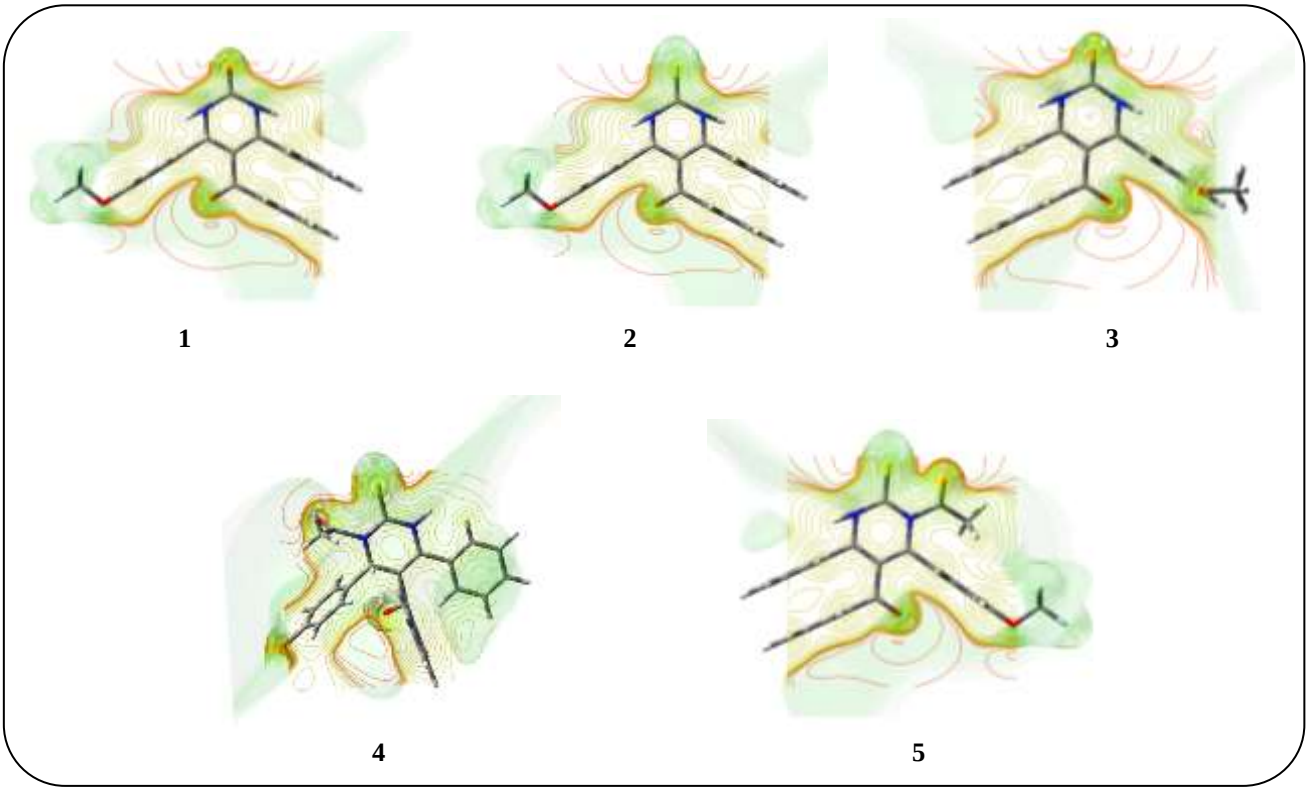

Fig. 6: MEPs of all molecules.

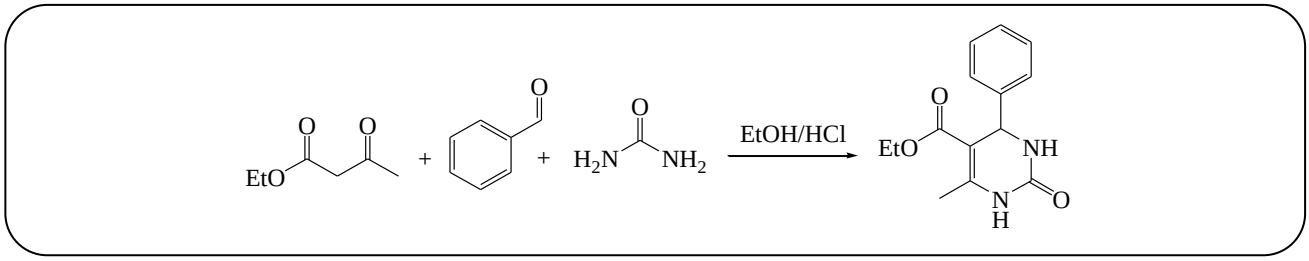

Scheme 3: The original Biginelli reaction.

for the electrophilic and nucleophilic attack as well as hydrogen-bonding interactions in the molecules. MEPs at the B3LYP/6-31+G (d, p) for all molecules were obtained and given in Fig. 6. In the figure, the negative (red) regions of MEP were related to electrophilic reactivity and the positive (blue) regions to nucleophilic reactivity.

CONCLUSIONS

The original Biginelli reaction is the three-component one-pot condensation of benzaldehyde, ethyl acetoacetate, and urea in the presence of strong acid as a catalyst in ethanol to give substituted 3,4-dihydropyrimidin-2(1*H*)-one (Scheme 3).

In this work, the pyrimidine derivatives were synthesized *via* the Biginelli reaction with a catalytic amount of MIL-101 in good yields (75-80%). All new structures were determined by using FT-IR, $^{1}H/^{13}C$ NMR, and elemental analyses. The compounds were investigated as corrosion inhibitors using density functional theory (DFT) at the level of B3LYP/6-31G (d, p).

As presented in Tables 2, 3 the compound which have the lowest energetic gap is compounds **4** and **5**. This lower gap allows it to be the softest molecule.

The two properties like I (potential ionization) and A (affinity) are so important, that the determination of these two properties allows us to calculate the absolute electronegativity (χ) and the absolute hardness (η). These two parameters are related to the one-electron orbital energies of the HOMO and LUMO respectively. Compounds **4** and **5** have the lowest value of the potential ionization (I), so they will be the better electron donor. Compounds **4** and **5** have the largest value of the affinity (A), so it is the better electron acceptor. The chemical reactivity varies with the structure of molecules.

The chemical hardness (softness) values of compounds **4** and **5** are lesser (greater) among all the molecules. Thus, compounds **4** and **5** are found to be more reactive than all the compounds. The value of ω for compounds **4** and **5** indicates that there is a stronger nucleophile than all other compounds.

The increase in inhibitory performance is due to more coverage of the metal surface because of the adsorption of the pyrimidine derivatives molecules onto the steel surface, which finally reduced the attack of acid. This finding suggests that the molecular structure of pyrimidine derivative molecules has a great influence on the inhibition efficiency values. In this study, the inhibitor molecules had π electrons in the aromatic ring and non-bonding electrons on the heteroatoms, such as oxygen, sulfur, and nitrogen, which helped the inhibitor to adsorb onto the steel surface. The number of electron-donating functional groups could also affect the adsorption tendency of the inhibitor, i.e., with more electron-donating functional groups, the adoption would be stronger and the inhibition efficiency would be higher. Thus, in the present case, compounds **4** and **5** had the highest protection ability due to the presence of an extra acetyl group. Therefore, the inhibition efficiency order was **4**=**5**>**3**-**1**.

According to all of the calculations, compounds **4** and **5** appear to be good inhibitors for corrosion than other molecules.

Acknowledgments

The authors would like to thank Dr. Mehmet Zahmakiran for the synthesis of mil101.

Received : Mar. 19, 2021 ; Accepted : Jun. 14, 2021

REFERENCES

[1] Biginelli P., Synthesis of 3,4-Dihydropyrimidin-2(1H)-Ones, *Gazz.Chim. Ital.*, **23**: 360 (1893).

[2] Akbas E., Berber I., Akyazi I., Anil B., Yildiz E., Microwave-assisted Synthesis of Tetrahydropyrimidines *via* Multicomponent Reactions and Evaluation of Biological Activities, *Letters in Organic Chemistry.*, **8(9)**: 663 (2011).

[3] Aslanoglu F., Akbas E., Studies on Reactions of Pyrimidine Compounds: Synthesis and Reactions of 5-benzoyl-4, 6-diphenyl-1, 2, 3, 4-tetrahydro-2-thioxopyrimidine, *Phosphorus, Sulfur, and Silicon and the Related Elements.*, **182**: 1589 (2007).

[4] Akbas E., Aslanoglu F., Studies on Reactions of Pyrimidine Compounds Microwave-Assisted Synthesis of 1,2,3,4-Tetrahydro-2- Thioxopyrimidine Derivatives, *Phosphorus, Sulfur, and Silicon and the Related Elements.*, **183**: 82 (2007).

[5] Kappe C.O., 100 Years of the Biginelli Dihydropyrimidine Synthesis, *Tetrahedron*, 49: 6937 (1993).

[6] Akbas E., Aslanoglu F., Anıl B., Şener A., A simple One-Pot Synthesis of 1,2,3,4-tetrahydro-2-thioxopyrimidine Derivatives, *J.Heterocyclic Chem.*, **45**: 1457 (2008).

[7] Akbas E., Sahin E., Yildiz E., Anil B., Akyazi İ., Microwave-Assisted Synthesis of New Dihydropyrimidine Derivatives and Mechanism of the Reactions, *Letters in Organic Chemistry*, **10**: 651 (2013).

[8] Atwal K.S., Swanson B.N., Unger S.E., Floyd D.M., Moreland S., Hedberg A., O'Reilly B.C., Dihydropyrimidine Calcium Channel Blockers. 3. 3-Carbamoyl-4-aryl-1,2,3,4-tetrahydro-6-methyl-5-Pyrimidinecarboxylic Acid Esters as Orally Effective Antihypertensive Agents, *J. Med. Chem.*, **34**: 806 (1991).

[9] Janis R.A., Silver P.J., Toggle D.J., Drug Action and Cellular Calcium Regulation Triggle, *Adv. Drug Res.*, **16**: 309 (1987).

[10] Akbas E., Ekin S., Ergan E., Karakus Y., Synthesis, DFT Calculations, Spectroscopy and in Vitro Antioxidant Activity Studies on 4-Hydroxyphenyl Substituted Thiopyrimidine Derivatives, *Journal of Molecular Structure*, **1174**: 177-183 (2018).

[11]Hu E.H., Sidler D.R., Dolling U.H., Unprecedented Catalytic Three Component One-Pot Condensation Reaction: An Efficient Synthesis of 5-Alkoxycarbonyl- 4-aryl-3,4-dihydropyrimidin-2(1H)-ones, *J. Org. Chem.*, 63: 3454-3457 (1998).

[12]Liu C., Wang J., Li Y., One-pot Synthesis of 3,4-dihydropyrimidin-2(1H)-(thio)ones Using Strontium(II) Nitrate as a Catalyst, *J. Mol. Catal. A: Chem.*, **258**: 367-370 (2006).

[13] Maradur S.P., Gokavi G.S., Heteropoly Acid Catalyzed Synthesis of 3,4-dihydropyrimidin-2(1H)-ones, *Catal. Commun.*, **8**: 279-284 (2007).

[14] Juan-Alcaniz J., Ramos-Fernandez E.V., Lafont U., Gascon J., Kapteijn F., Building MOF Bottles Around Phosphotungstic Acid Ships: One-Pot Synthesis of Bi-Functional Polyoxometalate-MIL-101 Catalysts, *J. Catal*., **269**: 229-241 (2010).

[15] Hu X., Lu Y., Dai F., Liu C., Liu Y., Host-Guest Synthesis and Encapsulation of Phosphotungstic Acid in MIL-101 via "Bottle Around Ship": An Effective Catalyst for Oxidative Desulfurization, *Microporous Mesoporous Mater*., **170**: 36-44 (2013).

[16] Maksimchuk N.V., Kovalenko K.A., Arzumanov S.S., Chesalov Y.A., Mel-gunov M.S., Stepanov A.G., Fedin V.P., Kholdeeva O.A., Hybrid polyoxotungstate/MIL-101 materials: Synthesis, Characterization, and Catalysis of H_2O_2-Based Alkene Epoxidation, *Inorg. Chem.*, **49**: 2920-2930 (2010).

[17] Zang Y., Shi J., Zhao X., Kong L., Zhang F., Zhong Y., Highly Stable Chromium(III) Terephthalate Metal Organic Framework (MIL-101) Encapsulated 12-Tungstophosphoric Heteropolyacid as a Water-Tolerant Solid Catalyst for Hydrolysis and Esterification, *React. Kinet. Mech. Catal.*, **109**: 77-89 (2013).

[18] Mrinal S., Diganta B., Lakshi S., Keggin Type Phosphotungstic Acid Encapsulated Chromium (III) Terephthalate Metal Organic Framework as Active Catalyst for Biginelli Condensation, *Applied Catalysis A: General*, **505**: 501-506 (2015).

[19] Akbas E., Levent A., Gumus S., Sumer M.R., Akyazi I., Synthesis of Some Novel Pyrimidine Derivatives and Investigation of Their Electrochemical Behavior, *Bull. Korean Chem. Soc.*, **31**: 3632 (2010).

[20] Rasheeda K., Alva V.D.P., Krishnaprasad P.A., Samshuddin S., Pyrimidine Derivatives as Potential Corrosion Inhibitors for Steel in Acid Medium – An Overview, *Int. J. Corros. Scale Inhib*., **7**: 48 (2018).

[21] Samshuddin S., Narayana B., Yathirajan H. S., Gerber T., Hosten E., Betz R., 4-Meth-oxy-4-methyl-6-phenyl-1,3-diazinane-2-thione, *Acta Crystallogr., Sect. E: Struct. Rep. Online*, **68**: 3271 (2012).

[22] Kapustin Y.I., Kholodkova A.G., Vagramyan T.A., Investigating Inhibitor Influence on Pickling Tin Metal Resist from Copper Conductors of Printed Circuit Boards, *International Journal of Corrosion and Scale Inhibition*, **7**: 1 (2018).

[23] Akbas E., Ruzgar A., Sahin E., Ergan E., A Green Protocol for Simple One- pot Synthesis of New Pyrimidine Derivatives Both Microwave Irradiation and Conventional Heating: Reactions, Characterization, and Theoretical Calculations, *J. Heterocycl. Chem*., **3**: 1003 (2019).

[24] *Gaussian 09, Revision E.01*, Gaussian Inc., Wallingford CT, 2009.

[25] Gece G., Theoretical Evaluation of the Inhibition Properties of Two Thiophene Derivatives on Corrosion of Carbon Steel In Acidic Media, *Mater. Corros.*, **64**: 940 (2013).

[26] Shojaie F., Baghini N.M., Molecular Dynamics and Density Functional Theory Study on the Corrosion Inhibition of Austenitic Stainless Steel in Hydrochloric Acid By Two Pyrimidine Compounds, *Int. J. Ind. Chem.*, **6**: 297 (2015).

[27] Rigaku/MSC, Inc., 9009 new Trails Drive, TheWoodlands, TX 77381.

[28] Sheldrick G.M., SHELXS-97 and SHELXL-97, Program for Crystal Structure Solution and Refinement, University of Göttingen, Germany (1997).

[29] Folkers K., Johnson T.B., Researches on Pyrimidines. CXXXVI. The Mechanism of Formation of Tetrahydropyrimidines by the Biginelli Reaction, *J. Am. Chem. Soc.*, **55**: 3784-3791(1933).

[30] Sweet F., Fissekis J.D., Synthesis of 3,4-dihydro-2(1H)-pyrimidinones and the mechanism of the Biginelli reaction, *J. Am. Chem. Soc*., **95**: 8741-8749 (1973).

[31] Kappe C.O., A Reexamination of the Mechanism of the Biginelli Dihydropyrimidine Synthesis. Support for an *N*-Acyliminium Ion Intermediate, *J. Org. Chem.* **62(21)**: 7201-7204 (1997).

[32] Ertas I.E., Gülcan M., Bulut A., Yurderi M., Zahmakiran M., Metal-Organic Framework (MIL-101) Stabilized Ruthenium Nanoparticles: Highly Efficient Catalytic Material in the Phenol Hydrogenation, *Microporous and Mesoporous Materials*, **226**: 94-103 (2016).

[33] Frisch M.J., et al., Gaussian 09, Revision A.02. Gaussian, Inc., Wallingford, CT, (2009).

[34] Becke A.D., Density- Functional Thermochemistry. III. The Role of Exact Exchange, *J. Chem. Phys.*, **98**: 5648-5652 (1993).

[35] Lee C.T., Yang W., Parr R.G., Development of the Colle-Salvetti Correlation-Energy Formula into a Functional of the Electron Density, *Phys. Rev. B.*, **37**: 785-789 (1988).

[36] Stephens P.J., Devlin F.J., Chabalowski C.F., Frisch M.J., Ab Initio Calculation of Vibrational Absorption and Circular Dichroism Spectra Using Density Functional Force Fields, *J. Phys. Chem.*, **98**: 11623-11627 (1994).

[37] Lee C., Sosa C., Local Density Component of the Lee–Yang–Parr Correlation Energy Functional, *The Journal of Chemical Physics.*, **100**: 9018 (1994).

[38] Stango S.A.X., Vijayalakshmi U., Studies on Corrosion Inhibitory Effect and Adsorption Behavior of Waste Materials on Mild Steel in Acidic Medium, *J. Asian Ceram. Soc.*, **6**: 20 (2018).

[39] Gece G., The Use of Quantum Chemical Methods in Corrosion Inhibitor Studies, *Corros. Sci.*, **50**: 2981 (2008).

[40] Popova A., Christov M., Zwetanova A., Effect of the Molecular Structure on the Inhibitor Properties of Azoles on Mild Steel Corrosion in 1 M Hydrochloric Acid, *Corros. Sci.*, **49**: 2131 (2007).

[41] Parr R. G., Szentpaly L., Liu S., Electrophilicity Index, *J. Am. Chem. Soc.*, **121**: 1922 (1999).

[42] Chattaraj P. K., Sarkar U., Roy D. R., Electrophilicity Index, *Chem. Rev.* **106**: 2065 (2006).

[43] Farley C., Bhupathiraju N.V.S. D.K, John B.K., Drain C.M., Tuning the Structure and Photophysics of a Fluorous Phthalocyanine Platform, *J. Phys. Chem. A*, **120**: 7451 (2016).

[44] Becke A. D., Density- Functional Thermochemistry. I. The Effect of the Exchange- Only Gradient Correction, *J. Chem. Phys*., **96**: 2155 (1992).

[45] Becke A. D., Density- Functional Thermochemistry. III. The Role of Exact Exchange, *J. Chem. Phys*., **98**: 5648 (1993).